Hybrid control scheme for a half-bridge inverter

Carolina Albea-Sanchez, Oswaldo Lopez Santos, David A Zambrano Prada, Francisco Gordillo, Germain Garcia

Hybrid control scheme for a half-bridge inverter

C. Albea [*] **O. Lopez Santos** [**] **D. A. Zambrano Prada** [**]
F. Gordillo [***] **G. Garcia** [****]

[*] *LAAS-CNRS, Université de Toulouse, UPS, France (e-mail: calbea@laas.fr).*
[**] *Universidad de Ibagué, Colombia, (e-mail: oswaldo.lopez,david.zambrano@unibague.edu.co).*
[***] *Universidad de Sevilla, Spain (e-mail: gordillo@us.es).*
[****] *LAAS-CNRS, Université de Toulouse, INSA, France (e-mail: garcia@laas.fr).*

Abstract: This paper presents a control law based on Hybrid Dynamical Systems (HDS) theory for electronic inverters. This kind of systems are very suited for the use of such theory since they combine both kind of signals: continuous (voltages and currents) and discrete (on-off state of switches). Unlike previous applications of HDS to power converters, the studied problem can be considered as a tracking problem since the objective is to generate a desired ac voltage from a dc source. The effectiveness of the resultant control law is validated by means of simulations and experiments.

Keywords: Hybrid dynamical systems, output regulation, switching variables, inverters, optimality.

1. INTRODUCTION

The control of power converters is characterized by the fact that the input signals are discrete, since they are the on-off state of switching devices, while the rest of signals, including the ones to be controlled, are continuous. Therefore, hybrid dynamical systems (HDS) framework is suitable for modelling and controlling this kind of systems. Nevertheless, there are still very few applications of HDS to power converters. Most of the methods for the control of power converters use an averaged model in which the discrete signals are averaged during each sampling period and, thus, are considered continuous signals. Based on the averaged model, continuous control laws are obtained. The resultant continuous control signals are discretized using the so-called modulation stage, for which different methods exist [Franquelo et al. 2008, Rodriguez et al. 2009]. Nevertheless, there exist other families of methods that explicitly consider the discrete nature of the control signals. These families include direct torque and flux controllers for motor drives [Rodríguez et al. 2004], and model predictive control [Kouro et al. 2009].

The HDS framework was firstly applied to electronic converters in 2003 [Senesky et al. 2003] and after that more applications have appeared [Sreekumar and Agarwal 2008, Deaecto et al. 2010, Albea et al. 2015]. All these applications consider dc-dc converters, whose objective, from the control theory point of view, is to stabilize an operating point. Nevertheless, in other electronic converters is usual to work with ac and thus, the problem is more involved. When ac voltage is to be generated, as is the case of inverters, the objective is to track a sinusoidal reference. Likewise, the advantage of using this HDS framework is to reduce switching frequency, while a optimality level is guaranteed.

In this paper, the control of the half-bridge inverter is addressed using HDS theory. The model is developed in Sect. 2 while the hybrid control law is obtained in Sect. 3. In Sect. 4 a procedure for parameter tuning is presented in order to improve the converter performance. Simulations are presented in Sect. 5, and experiment results are presented in Sect. 6. The paper closes with a section of conclusions and future work.

2. INVERTER MODEL

Let us consider a half-bridge converter dc-ac fed by a constant voltage source, V_{in}, and composed of a load filter, L, C_0, a purely resistive load, R_0, and a parasite resistance, R_{LS}, that encompasses the inductance and switching energy dissipation. It is shown in Fig. 1. The system differential equations can be written as

$$\frac{d}{dt}\begin{bmatrix} i_L(t) \\ v_C(t) \end{bmatrix} = \begin{bmatrix} -\frac{R_{LS}}{L} & -\frac{1}{L} \\ \frac{1}{C_0} & -\frac{1}{R_0 C_0} \end{bmatrix} \begin{bmatrix} i_L(t) \\ v_C(t) \end{bmatrix} + \begin{bmatrix} \frac{V_{in}}{L} \\ 0 \end{bmatrix} u \quad (1)$$

where i_L is the inductance current v_C is the capacitor voltage, and they are the two state variables. On the other side, $u = U_1 - U_2 \in \{-1, 1\}$ is the control input which represents two operating modes. The first one, $u = -1$, corresponds to $U_1 = 0$ (U_1 OFF) and $U_2 = 1$ (U_2 ON). And the second one, $u = 1$, corresponds to $U_1 = 1$ (U_1 ON) and $U_2 = 0$ (U_2 OFF). Note, that due to the converter topology v_C and i_L are alternating voltage and current, respectively.

Assumption 1. Consider that the capacitors C_1 and C_2 are large enough, such that the voltage ripples are negligible and, therefore, they are not considered in system (1).

From a practical point of view, the general control objective of this class of inverter is to stabilize system (1) in a desired oscillatory trajectory. That means, to control the inverter such that its output voltage asymptotically tracks a sinusoidal reference.

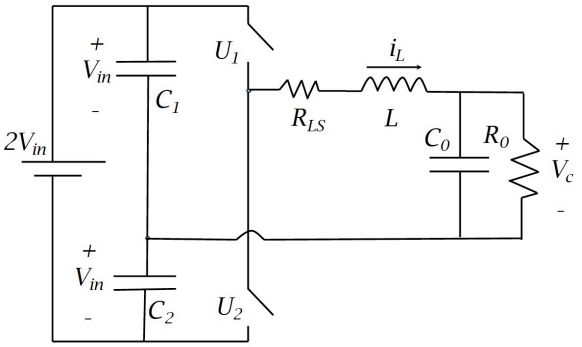

Fig. 1. Inverter half-bridge.

For this deal let us consider system (1) described by the following state-space equation:

$$\dot{x} = Ax + Bu \tag{2}$$

where $x = [i_L \ v_C]^T$ are continuous-time variables representing the internal states and, $u \in \{-1, 1\}$ is the discrete-time variable depicting the control input.

The practical objective mentioned above means to control the inverter to impose a desired trajectory on v_C defined by

$$v_{C_d}(t) = V_{max} \sin(\omega t). \tag{3}$$

A simple circuit analysis shows that if in steady state $v_C = v_{C_d}$, the current i_L in the inductance is given by

$$i_{L_d}(t) = C_0 \omega V_{max} \cos(\omega t) + \frac{V_{max}}{R_0} \sin(\omega t). \tag{4}$$

V_{max} is the desired amplitude of the voltage through the load R_0. To impose such a behavior, let us drive system (2) by an exogenous input $z \in \mathbb{R}^2$ generated by the next stable time-invariant exosystem:

$$\dot{z} = \begin{bmatrix} 0 & -\omega \\ \omega & 0 \end{bmatrix} z = \Theta z \qquad z(0) = \begin{bmatrix} 0 \\ V_{max} \end{bmatrix}. \tag{5}$$

Remark 1. From (5) it is simple to see that for all t

$$z_1^2(t) + z_2^2(t) = V_{max}^2.$$

Define the compact set

$$\Phi = \{z_1^2 + z_2^2 = V_{max}^2, \ (z_1, z_2) \in \mathbb{R}\}.$$

The dynamics of the overall system is defined by

$$\begin{aligned} \dot{x} &= Ax + Bu, \\ \dot{z} &= \Theta z, \\ e &= Cx + Dz = x - \Pi z, \end{aligned} \tag{6}$$

where $e \in \mathbb{R}^2$ is the tracking error, $C \in \mathbb{R}^2$ is the identitiy matrix, $D = \Pi$ being Π defined from (3) and (4) as:

$$\Pi = \begin{bmatrix} \omega C_0 & \dfrac{1}{R_0} \\ 0 & 1 \end{bmatrix}.$$

Let us denote as Γ the solution of the following algebraic equation

$$A\Pi + B\Gamma = \Pi\Theta. \tag{7}$$

A simple calculation shows that

$$\Gamma = \begin{bmatrix} \dfrac{\omega L}{R_0 V_{in}} + \dfrac{w R_{LS} C_0}{V_{in}} & \left(\dfrac{1}{L} - C_0 \omega^2 + \dfrac{R_{LS}}{L R_0} \right) \dfrac{L}{V_{in}} \end{bmatrix}.$$

Remark 2. Equation (7) is the well known "regulator equation", [Francis 1977, Serrani et al. 2001]. In addition, we remark that we have

$$C\Pi + D = 0.$$

Then, from (6) and following (7), the tracking error dynamic is given by

$$\begin{aligned} \dot{e} = \dot{x} - \Pi \dot{z} &= Ax + Bu - \Pi\Theta z \\ &= Ax + Bu - A\Pi z - B\Gamma z \\ &= Ae + Bv. \end{aligned} \tag{8}$$

where

$$v = u - \Gamma z. \tag{9}$$

Assumption 2. z_2 is supposed to be measurable as a reference in such a way that the inverter will produce a voltage with the same amplitude, frequency and phase. Then, z_1 can be internally reconstructed, as it is shown in Fig. 2.

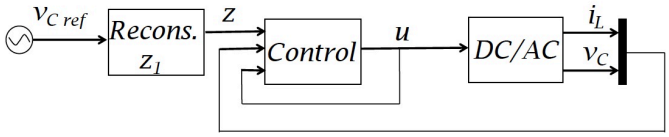

Fig. 2. Block diagram of the controlled inverter.

The problem in this paper can now be stated.

Problem 1. To design a control law v (or equivalently u) such that for any initial condition $e(0) \in \mathbb{R}^2$:

- the trajectory of (8) is bounded,
- and

$$\lim_{t \to \infty} e(t) = 0.$$

To solve Problem 1, we will use the main idea proposed in [Albea et al. 2015], formulating the problem under an hybrid dynamical framework following the theory given in [Goebel et al. 2012], wherein continuous-time behavior follows the evolution of the voltage and current in (1), and the discrete-time behavior captures the switch of the control signal u. Likewise, we remark that the problem is an output regulation problem and the idea here is also inspired by the work in [Francis 1977, Serrani et al. 2001].

3. HYBRID MODEL AND PROPOSED CONTROL LAW

Let us recall that error dynamics are described by

$$\begin{aligned} \dot{e} &= Ae + Bv, \\ \dot{z} &= \Theta z, \end{aligned} \tag{10}$$

where the available input v given in (9) is composed of a continuous-time signal Γz and a switching signal u, which can achieve a logical mode between 2 possible cases

$$u \in \{-1, 1\}.$$

This paper focuses on the design of a control law for the switching signal u, in order to ensure suitable convergence

properties of the inverter error variable e to 0. Following the works shown in [Albea et al. 2015, Deaecto et al. 2010, Liberzon and Morse 1999], we represent in the following assumption a necessary and sufficient condition that characterizes the existence of a suitable switching signal inducing $e = 0$.

Assumption 3. Given a matrix $Q = Q^T > 0$, there exists a matrix $P = P^T > 0$ such that:

- the matrix A verifies
$$A^T P + PA + 2Q < 0, \tag{11}$$
- there exist two scalar $\lambda_1, \lambda_{-1} \in [0, 1]$ satisfying $\lambda_1, +\lambda_{-1} = 1$, such that for a given $z \in \mathbb{R}^2$
$$\lambda_1 - \lambda_{-1} - \Gamma z = 0. \tag{12}$$

Note that the existence of $e = 0$ for (10) is given in Assumption 3, allowing to be $v = 0$ through a convex combination of the two operating modes of u as follows

$$v = 1 \cdot \lambda_1 + (-1) \cdot \lambda_{-1} - \Gamma z.$$

Likewise, we remark that $e = 0$ allows a Krasovskii solution and even a Fillipov solution, because (12) means that in $e = 0$ the signal is a periodic sequence of arbitrarily small period T, spending a time equal to $\lambda_1 T$ in mode $u = 1$, and $\lambda_{-1} T$ in mode $u = -1$. Likewise, if Assumption 3 does not hold, such a signal does not exist because any arbitrary switching signal can only generate an equivalent action on $\dot{e}$ corresponding to a convex combination obtained with each mode (namely, equation (12)).

In order to present the proposed control law, consider the following HDS model:

$$\mathcal{H} : \begin{cases} \begin{bmatrix} \dot{e} \\ \dot{z} \\ \dot{v} \end{bmatrix} = f(e, z, v), & (e, z, v) \in \mathcal{C} \\ \begin{bmatrix} e^+ \\ z^+ \\ v^+ \end{bmatrix} \in G(e, z), & (e, z, v) \in \mathcal{D}, \end{cases} \tag{13}$$

where G is a set-valued map representing the switching logic:

$$f(e, z, v) := \begin{bmatrix} Ae + Bv \\ \Theta z \\ -\Gamma\Theta z \end{bmatrix}$$

$$G(e, z) := \begin{bmatrix} e \\ z \\ \left(\underset{u \in \{-1,1\}}{\operatorname{argmin}} \; e^T P(Ae + B(u - \Gamma z)) \right) - \Gamma z \end{bmatrix} \tag{14}$$

and where the flow and jump sets $\mathcal{C}$ and $\mathcal{D}$ encompass, respectively, the regions in the (extended) space (e, z, v) where our switching strategy will continue with the current mode v when the states are in set $\mathcal{C}$ or will be require to switch to a new mode when the states are in set $\mathcal{D}$. If $(e, z, v) \in \mathcal{D}$ then u will switch according to G in (14) given the value of $v = u - \Gamma z$.

Based on the parameters P and Q introduced in Assumption 3, we select the following flow and jump sets:

$$\mathcal{C} := \{(e, z, v) : e^T P(Ae + Bv) \leq -\eta e^T Qe\} \tag{15}$$

$$\mathcal{D} := \{(e, z, v) : e^T P(Ae + Bv) \geq -\eta e^T Qe\}, \tag{16}$$

where $\eta \in (0, 1)$ is a useful design parameter allowing to achieve a trade-off between optimality level and switching frequency, as characterized below in Theorem 2.

Proposition 1. The hybrid dynamical system (13)–(16) satisfies the basic hybrid conditions [Goebel et al. 2012, Assumption 6.5], then it is well-posed.

Proof. To prove the hybrid basic conditions we see that the sets $\mathcal{C}$ and $\mathcal{D}$ are closed. Moreover f is a continuous function, thus it trivially satisfies outer semicontinuity and convexity properties. The map G is closed, therefore it also is outer semicontiunuous [Goebel et al. 2012, Lemma 5.1]. And, f and G are locally bounded. Finally, the second conclusion of the proposition comes from [Goebel et al. 2012, Theorem 6.30]. □

Now, we evoke Lemma in [Albea et al. 2015, Lemma 1], which is fundamental to stablish Theorem 1.

Lemma 1. Consider that all conditions of Assumption 3 are satisfied. Then, for each $e \in \mathbb{R}^2$,

$$\min_{u \in \{-1,1\}} e^T P(Ae + B(u - \Gamma z)) \leq -e^T Qe. \tag{17}$$

□

Proof. Define the compact set

$$\Lambda = \{\lambda_{-1}, \lambda_1 \in [0, 1] : \; \lambda_{-1} + \lambda_1 = 1\}.$$

Then, the following minimum is obtained at the extreme points:

$$\begin{aligned} &\min_{u \in \{-1,1\}} e^T P(Ae + Bu - B\Gamma z) \\ &= \min_{\lambda_1, \lambda_{-1} \in \Lambda} e^T P\left(Ae + B\lambda_1 - B\lambda_{-1} - B\Gamma z\right) \leq -e^T Qe, \end{aligned}$$

where in the last step we used relations (11) and (12) .

□

The switching signals generated by our solution will depend on Lemma 1. Indeed, Assumption 3 with (15) shows that unless $e = e^+ = 0$, the solution always jumps to the interior of the flow set $\mathcal{C}$ because

$$-e^T Qe < -\eta e^T Qe,$$

and $\eta < 1$. This fact, together with stability (ensuring boundedness of solutions) and the sector growth condition

$$|\dot{e}| = |\dot{x}| \leq |Ae| + |Bv| \leq \kappa_1 |e| + \kappa_2$$

with κ_1 and κ_2 positive constants, coming from the flow dynamics (10), implies that there is a uniform lower bound on the dwell time between each pair of consecutive resets before solutions approach $e = 0$. Note that, as in other cases, (see [Deaecto et al. 2010], for instance) the desired behaviour $e = 0$ is achieved with an arbitrarily fast switching. The essential difference in our approach is that during transient time the solution is characterized by relatively slow switching adjusted by η. The same paradigm was followed in [Theunisse et al. 2015] using very similar techniques but we focus here on a different class of systems.

Following up, we will establish uniform stability and convergence properties of the hybrid system (13)–(16) to the compact attractor

$$\mathcal{A} := \{(e, z, v) : e = 0, z \in \Phi, u \in \{-1, 1\}\}, \tag{18}$$

where the set Φ is defined in Remark 1.

Theorem 1. Under Assumptions 2,3 the attractor (18) is uniformly globally asymptotically stable (UGAS) for hybrid system (13)–(16).

Proof. Let us take the Lyapunov function candidate

$$V(e,z)=\frac{e^TPe}{2}.$$

In the flow set, $\mathcal{C}$, using its definition in (15), we have

$$\langle \nabla V(e,z), f(e,z,v)\rangle = e^TP(Ae+Bv) \leq -\eta e^TQe \quad (19)$$

Across jumps we trivally get:

$$V(e^+)-V(e)=\frac{1}{2}\left\{e^TPe-e^TPe\right\}=0. \quad (20)$$

because $e^+=e$.

Uniform global asymptotic stability is then shown applying [Prieur et al. 2014, Theorem 1]. In particular, since the distance of e to the attractor (18) is defined by $|e|_{\mathcal{A}}=|e|$, we have that [Prieur et al. 2014, eq. (6)] holds from the structure of V and from (19) and (20). [Prieur et al. 2014, Theorem 1] also requires building the restricted hybrid system $\mathcal{H}_{\delta,\Delta}$ by intersecting $\mathcal{C}$ and $\mathcal{D}$ with the set

$$S_{\delta,\Delta}=\{(e,z,v):|e|\geq\delta \quad \text{and} \quad |e|\leq\Delta\}$$

and then proving (semi-global) practical persistence flow for $\mathcal{H}_{\delta,\Delta}$, for each fixed values of (δ,Δ). In particular, practical persistent flow amounts to showing that there exists $\gamma\in\mathcal{K}_\infty$ and $M\geq 0$, such that, all solutions to $\mathcal{H}_{\delta,\Delta}$ satisfy

$$t\geq\gamma(j)-M, \qquad \forall t\in\bigcup_{j\in\mathrm{dom}_j\,\xi} I^j\times\{j\} \quad (21)$$

(see [Prieur et al. 2014] for details). To establish (21), notice that after each jump, from the definition of G in (14) and from property (17) (in Lemma 1), we have

$$e^T(Ax+Bv^+)\leq -e^TQe<-\eta e^TQe, \quad (22)$$

where we used the fact that $\eta<1$ and that $(0,z,v)\notin S_{\delta,\Delta}$. Therefore, if any solution to $\mathcal{H}_{\delta,\Delta}$ performs a jump from $S_{\delta,\Delta}$, it will remain in $S_{\delta,\Delta}$ (because e remains unchanged) and then, from (16), it jumps to the interior of the flow set $\mathcal{C}\cap S_{\delta,\Delta}$. Moreover, from the strict inequality in (22), then all non-terminating solutions must flow for some time and since $\mathcal{C}\cap S_{\delta,\Delta}$ is bounded, there is a uniform dwell-time $\rho(\delta,\Delta)$ between each pair of consecutive jumps. This dwell-time (δ,Δ) clearly implies [Prieur et al. 2014, eq. (4)] with the class $\mathcal{K}_\infty$ function $\gamma(j)=\rho(\delta,\Delta)j$ and $M=1$. Then, all the assumptions of [Prieur et al. 2014, Theorem 1] hold and UGAS of $\mathcal{A}$ is concluded. □

Corollary 1. The hybrid dynamical system (13)–(16) is UGAS and is robust with respect to the presence of small noise in the state, unmodeled dynamics, and spatial regularization to relax the rate of switching, because the attractor (18) is compact.

Proof. From Theorem 1, we prove that the hybrid dynamic system is UGAS, and from Proposition 1 we see that it is well-posed. Moreover, as the attractor (18) is compact then it is robustly $\mathcal{KL}$ asymptotically stable in a basin of attraction. □

Remark 3. Note that according to Theorem 1 system (13)–(16) may exhibit a Zeno behaviour when $e\to 0$, and consequently an infinitely fast switching may be expected, which is not acceptable in practice. This will be practically avoided later introducing an additional dwell-time logic to obtain a temporal-regularisation of the dynamics, thereby weakening asymptotic convergence into practical convergence.

4. OPTIMALITY AND PARAMETERS TUNING

Once that UGAS of the attractor is established for our solution, we focus on providing a suitable performance guarantee by reducing the energy cost, current peaks and response time, for instance. For this goal we apply the same paradigm shown in Albea et al. [2015] for a hybrid context applied to switched systems.

Following the hybrid theory given in [Goebel et al. 2012], we consider that the domain of a a solution ξ corresponds to a finite or infinite union of intervals defined as

$$\mathrm{dom}\,\xi=\bigcup_{j\in\mathrm{dom}_j\,\xi} I^j\times\{j\}, \quad (23)$$

with $I^j=[t_j,t_{j+1}]$ being a bounded time interval of the ordinary continuous time t and having the discrete-time (or "jump times") t_j as extremes, where j represents the number of switches; or $I^j=[t_j,+\infty)$ being a last unbounded interval .

Let adapt the notation $\mathrm{dom}_j\,\xi:=\{j\in\mathbb{Z}:\ (t,j)\in\mathrm{dom}\,\xi,\ \text{for some } t\in\mathbb{R}\}$ and represent an LQ performance metric focusing on the flows of the inverter, using the expression

$$J(\xi):=\sum_{k\in\mathrm{dom}_j\,\xi}\int_{t_k}^{t_{k+1}} x^TC^TCx d\tau, \quad (24)$$

where $\xi=(x,z,v)=(e,z,v):\mathrm{dom}\,\xi\to\mathbb{R}^n\times\mathbb{R}^n\times\mathbb{R}^n$ is a solution to hybrid system (13)–(16), $Ce(t,j)$ for all $(t,j)\in\mathrm{dom}\,\xi$.

The following theorem guarantees the performance cost (24) for our hybrid system.

Theorem 2. Consider hybrid system (13)–(16) satisfying Assumption 2,3. If

$$C^TC\leq Q, \quad (25)$$

then the following bound holds along any solution $\xi=(e,z,v)$ of (13)–(16):

$$J(\xi)\leq\eta^{-1}e(0,0)^TPe(0,0), \quad (26)$$

where $e(t,j)=x(t,j)-x_{ss}$, for all $(t,j)\in\mathrm{dom}(\xi)$.

Proof. To prove the optimality property in (26), consider any solution $\xi=(e,z,v)$ to $\mathcal{H}$. Then for each $(t,j)\in\mathrm{dom}\,\xi$ and denoting $t=t_{j+1}$ to simplify notation, we have from (19)

$$
\begin{aligned}
&V(e(t,j)) - V(e(0,0)) \\
&= \sum_{k=0}^{j} V(e(t_{k+1},k)) - V(e(t_k,k)) \\
&= \sum_{k=0}^{j} \int_{t_k}^{t_{k+1}} \langle \nabla V(e(\tau,k)), f(x(\tau,k),u(\tau,k)) \rangle d\tau \\
&\leq \sum_{k=0}^{j} \int_{t_k}^{t_{k+1}} -\eta e^T(\tau,k) Q e(\tau,k) d\tau \\
&\leq -\eta \sum_{k=0}^{j} \int_{t_k}^{t_{k+1}} e^T(\tau,k) C^T C e(\tau,k) d\tau, \qquad (27)
\end{aligned}
$$

where the last inequality comes from applying (25). Now, considering $\tilde{y}(\tau,k) = Ce(t,k)$, taking the limit as $t + j \to +\infty$ and using the fact that UGAS established in Theorem 1 implies $\lim_{t+j\to+\infty} V(e(t,j)) = 0$, we get from (27)

$$\eta J(\xi) \leq V(e(0,0)) = e(0,0)^T P e(0,0),$$

as to be proven. □

Remark 4. Note that for a given P and Q that satisfy (25), the guaranteed performance level is proportional to the inverse of $\eta \in (0,1)$. That means that large values of η (as close as possible to 1) in transient time are expected to drive to improved LQ performance along solutions.

On the other hand, note from the flow and jump sets in (15) and (16), that larger values of η (close to 1) correspond to strictly larger jump sets (and smaller flow sets), which reveals that solutions with larger values of η exhibit a larger switching frequency. In other words, through parameter η we can deal with a trade off between switching frequency and performance along solutions in transient time, affecting the level of guaranteed optimality given in (26).

4.1 Computation of P and Q

Now, we address the problem of the computation of parameters P, Q, following any class of optimization that reduces as much as possible the right hand side in bound (26). To this end, we select

$$Q = C^T C + \nu I, \qquad (28)$$

where $\nu > 0$ is a positive constant small enough, which must be selected different to zero if $C^T C \geq 0$ (as happens in our case in (2)), ensuring $Q > 0$ as well as restriction (25).

Once Q is selected, and noting that matrix A is Hurwitz, the following convex optimization expressed by the following linear matrix inequality always leads to a feasible solution

$$
\begin{aligned}
\min_{P=P^T>0} \ &\text{Trace}P, \text{ subject to:} \qquad (29) \\
&A^T P + P A^T \leq -2Q,
\end{aligned}
$$

and this optimal solution clearly satisfies (11).

5. SIMULATION

In this section, we validate in simulation the hybrid controller designed in this paper for the inverter given in (1). Following the optimality and parameters tuning given in [Albea et al. 2015, Section IV], we select the cost function J as follows:

$$\min_u \sum_{k\in \text{dom}_j(\xi)} \int_{t_k}^{t_{k+1}} \frac{\rho}{R_0}(v_C(\tau,k) - v_{C_d})^2 + R_{LS}(i_L(\tau,k) - i_{L_d})^2 d\tau,$$

where ρ is a positive scalar. Note that the constant parameters of each term express the weighted sum of the energy of the error signal of each state variable.

Likewise, we take $Q = \begin{bmatrix} R_{LS} & 0 \\ 0 & \dfrac{\rho}{R_0} \end{bmatrix}$.

Table 1. Simulation parameters

Parameter	Convention	Value	Units
DC input voltage	V_{in}	96	V
Rererence peak voltage	V_{max}	$220\sqrt{2}$	V
Nominal angular frequency	ω	$2\pi\,(50)$	rad/s
Inductor	L	50	mH
Output capacitor	C_0	200	μF
Load resistance	R_0	220	Ω
Estimated series resistance	R_{LS}	2	Ω

Now, from parameters given in Table 1 and from (3) and (4) we got the following desired behaviour

$$x_d = \begin{bmatrix} v_{c_d} \\ i_{L_d} \end{bmatrix} = \begin{bmatrix} 220\sqrt{2}\sin(2\pi 50 t) \\ 19.5\sin(2\pi 50 t + 86^\circ)) \end{bmatrix},$$

where it was applied the trigonometric relationship: $a\cos(x) + b\sin(x) = \sqrt{(a^2+b^2)}\sin(x - \text{atan}(\frac{b}{a}) + \frac{\pi}{2})$. Moreover, we take a sampling time $T_s = 10^{-6}s$, $\rho = 1000$ and

$$P = \begin{bmatrix} 9 & 0.07 \\ 0.07 & 0.04 \end{bmatrix}.$$

Simulations are performed in MATLAB/Simulink by using the HyEQ Toolbox [Sanfelice et al. 2013].

First, note that condition (11) is satisfied. Moreover, considering that Assumption 2 is satisfied (the voltage of the network is measured) we get to stabilize x in x_d in simulation, satisfying condition (12). Thus, from Theorem 1 the attractor (18) of the inverter guarantees UGAS. These properties can be appreciated from the simulations of Fig. 3 that shows the voltage and current evolutions of the controlled inverter with different values of η. Likewise, Fig. 4 shows the normalized switching frequency and cost function J to the maximum valued obtained in simulations in a time slot of the transient as a function of η. Note that, the cost function is reduced with larger values of η, on the contrary, the trend of the switching frequency is to grow with larger values of η. Thus we may give up a little on the level of optimality and suitably adjust the switching frequency, finding a satisfactory trade off between performance and switching frequency in $\eta = 0.4$, which corresponds at the intersection between the switching curve and the cost function for any given initial condition.

On the other hand, in Remark 3 we note that there is infinitely fast switching in the steady-state. In practice, this is not desired in terms of energy efficiency and reliability, since every switch dissipates energy and reduces the switch lifespan. This is not appreciated in Fig. 3 because we used a sampling time. If we want to avoid this infinitely

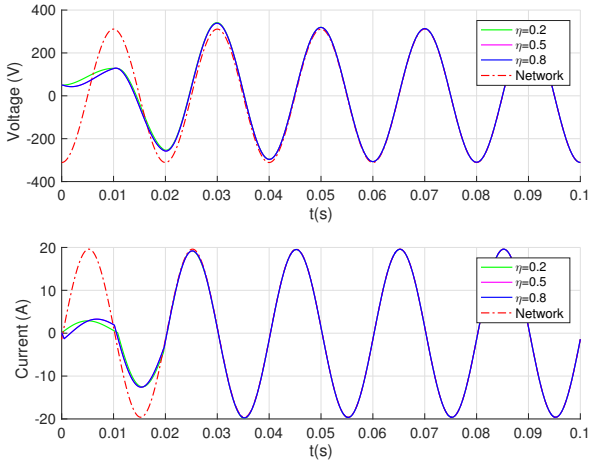

Fig. 3. Voltage and current evolution of the inverter.

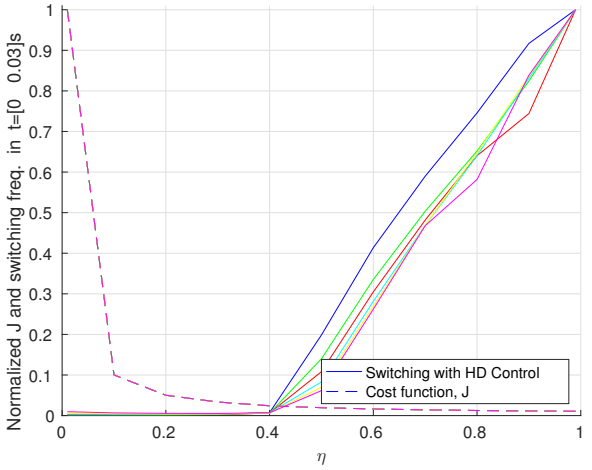

Fig. 4. Evolution of the normalized switching frequency (solid) and cost function J (dashed) w.r.t. η for different initial conditions in the inverter.

fast switching without the need to introduce a sampling time, we propose a space-regularisation through a dwell-time that separates the regions (15) and (16). For this aim, the flow and jump sets are

$$\mathcal{C} := \{(e, z, v) : e^T P(Ae + Bv) \leq -\eta e^T Qe \text{ or } V(e) \leq \eta_2\} \tag{30}$$

$$\mathcal{D} := \{(e, z, v) : e^T P(Ax + Bv) \geq -\eta e^T Qe \ \& \ V(e) \geq \eta_2\}, \tag{31}$$

being $\eta_2 > 0$ small enough and $\eta \in (0, 1)$. With these flow and jump maps, it is expected to achieve a reduction of switching in the steady-state as η_2 increase.

Some simulations are given in Fig. 5 with the practical hybrid system (13)–(14) with (30)–(31) and compared with the main hybrid system (13)–(16), which are equivalent with $\eta_2 = 0$. Note that the voltage evolution is essentially the same for different values of η_2. On the other hand, as was mentioned above, note that as η_2 is increased, it is expected a reduction of the switching frequency, which is consistent with the upper two plots of Fig. 6. For these simulations we chose $\eta = 0.4$.

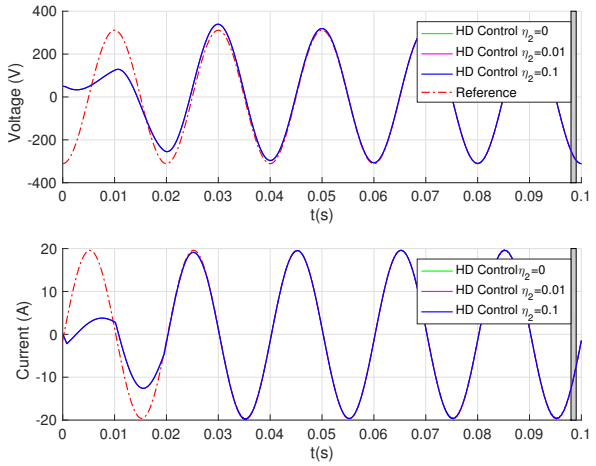

Fig. 5. Voltage and current evolution of the inverter and $\eta = 0.4$.

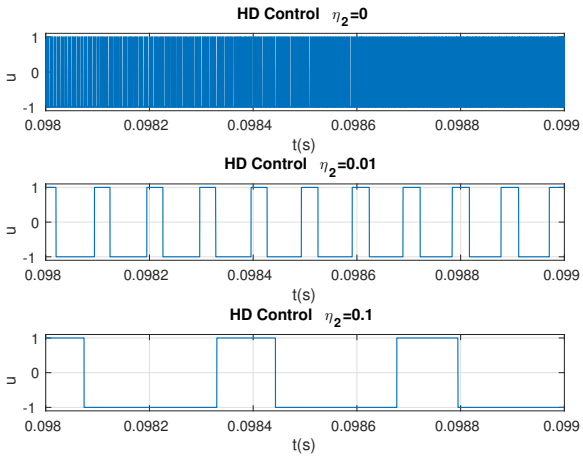

Fig. 6. Zoom of u in the inverter with $\eta = 0.4$.

6. EXPERIMENTAL RESULTS

In order to validate the proposed control, a scale laboratory prototype was built using parameters in Table 2. The nominal frequency of 400 Hz was selected considering its use in aircraft applications while the scale voltages was selected in order to have an inductor current similar to the case presented in simulation results. The half bridge uses two MOSFET IRFZ44 triggered using photo-coupled MOSFET drivers TLP350, one isolated closed-loop hall-effect transducer LV-20P measuring the output voltage and one isolated closed-loop hall-effect transducer CAS 15-NP measuring the inductor current, both sensors conditioning using analogue circuitry. The control algorithm was embedded in a Digital Signal Processor (DSP) TMS32028335 running with an externally generated sampling frequency of 51.2 kHz (128 times the output frequency).

From the parameters given in Table 2 and following (3) and (4), the two required synchronized references are given by:

Table 2. Experimental prototype parameters

Parameter	Convention	Value	Units
DC input voltage	V_{in}	5	V
Rererence peak voltage	V_{max}	15	V
Nominal angular frequency	ω	$2\pi\,(400)$	Rad/s
Input capacitors	$C_{1,2}$	22	mF
Inductor	L	1.05	mH
Output capacitor	C	150	μF
Load resistance	R_0	120	Ω
Estimated series resistance	R_{LS}	1	Ω

$$x_d = \begin{bmatrix} v_{C_d} \\ i_{L_d} \end{bmatrix} = \begin{bmatrix} 15\sin(2\pi 400t) \\ 5.65\sin(2\pi 400t + 83^\circ) \end{bmatrix} \tag{32}$$

Note that Assumption 1 is satisfied by the values of $C_{1,2}$. Moreover, the gains introduced by measurements and conditioning circuits are compensated internally into the DSP device. The selected value of η_2 for these experiments was 0.01 and $\eta = 0.04$. The matrices P and Q were computed as follows:

$$P = \begin{bmatrix} 4 & -0.05 \\ -0.05 & 10 \end{bmatrix}, \quad Q = \begin{bmatrix} 1 & 0 \\ 0 & 4.54 \end{bmatrix}. \tag{33}$$

The experimental set-up is composed by one oscilloscope Tektronix MSO2014B with conventional voltage probes, one differential voltage probe, and one isolated current probe Fluke i30s, one function generator Gwinstek AFG-2025 which is used to produce the sampling frequency of the DSP, one programmable DC source BK precision XLN6024 which is used to provide the input voltage of the converter and one power source BK Precision 1672 feeding the sensors and auxiliary circuitry. The Fig. 7 shows the prototype assembled with the measurement set-up.

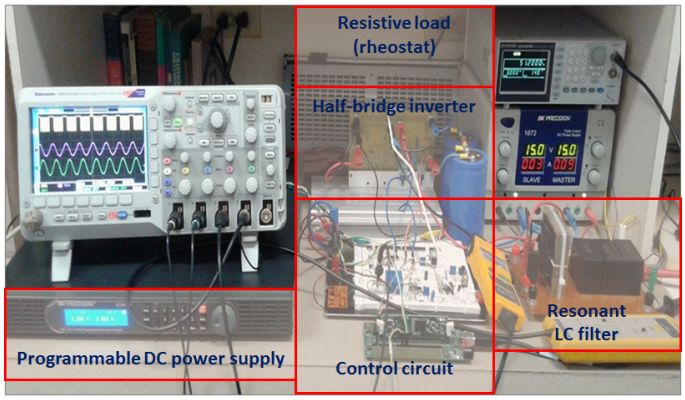

Fig. 7. Laboratory prototype and experimental set-up

As it is depicted in Fig. 8a, the output voltage reaches the stationary-state in frequency, phase and amplitude in less than five cycles (12.5 ms) showing the expected tracking of the sinusoidal reference. In Fig. 8b, the output voltage, inductor current and control signals captured with the oscilloscope are depicted. It is possible to observe the expected delay between the current and voltage waveform measured as $\theta \approx 82.6$.

7. CONCLUSIONS AND FUTURE WORK

In this work, we proposed a controller following a HDS framework for a dc-ac converter composed of continuous variables (current and voltage) and discrete variables

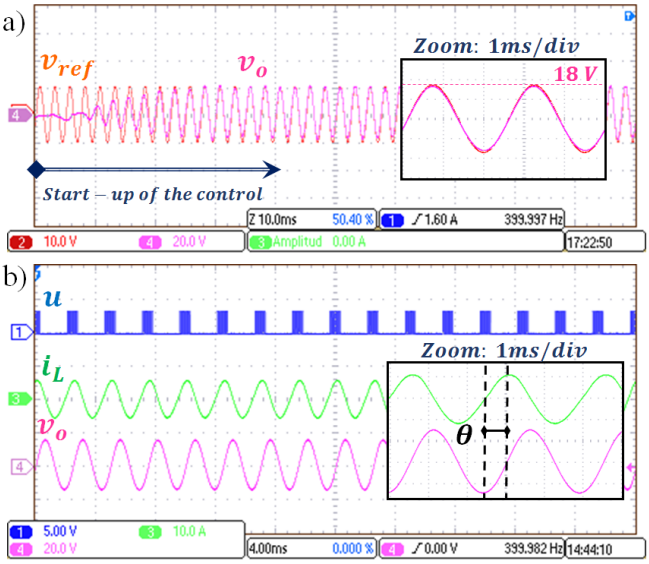

Fig. 8. Oscilloscope captures of the inverter signals: a) Signals at the start-up and synchronization interval; b) Signals at the stationary state

(state of switches), whose main problem is to track a sinusoidal reference. The main advantage of this method is to manage the switching frequency in the transient-state and guarantee a prescribed optimality level. Some simulations and experimental results validate our proposed hybrid control. Likewise, we shown that the switching frequency in the steady-state can be managed. In future work, we will establish that the compact attractor

$$\mathcal{A}_{\eta_2} =: \{V(e) \leq \eta_2, z \in \Phi, v \in \{-1, 1\}\}, \tag{34}$$

is UGAS for Hybrid system (13)–(14) with (30)–(31), and global practical asymptotic stability of the attractor (18) with respect to η_2. Another future work is to use this inverter to inject energy in the power grid, what means to synchronize the inverter in amplitude, frequency and phase with the power grid.

ACKNOWLEDGMENTS

This work has been partially funded under grants MINECO-FEDER DPI2013-41891-R and DPI2016-75294-C2-1-R.

REFERENCES

Albea, C., Garcia, G., and Zaccarian, L. (2015). Hybrid dynamic modeling and control of switched affine systems: application to dc-dc converters. In *proc. IEEE Conference on Decision and Control (CDC)*, 2264–2269.

Deaecto, G.S., Geromel, J.C., Garcia, F., and Pomilio, J. (2010). Switched affine systems control design with application to DC–DC converters. *IET control theory & applications*, 4(7), 1201–1210.

Francis, B.A. (1977). The linear multivariable regulator problem. *SIAM Journal on Control and Optimization*, 15(3), 486–505.

Franquelo, L.G., Rodriguez, J., Leon, J.I., Kouro, S., Portillo, R., and Prats, M.A. (2008). The age of multilevel converters arrives. *IEEE industrial electronics magazine*, 2(2), 28–39.

Goebel, R., Sanfelice, R., and Teel, A. (2012). *Hybrid Dynamical Systems: modeling, stability, and robustness.* Princeton University Press.

Kouro, S., Cortés, P., Vargas, R., Ammann, U., and Rodríguez, J. (2009). Model predictive control–A simple and powerful method to control power converters. *IEEE Trans. on Industrial Electronics*, 56(6), 1826–1838.

Liberzon, D. and Morse, A. (1999). Basic problems in stability and design of switched systems. *IEEE Control Systems Magazine*, 19(5), 59–70.

Prieur, C., Teel, A.R., and Zaccarian, L. (2014). Relaxed persistent flow/jump conditions for uniform global asymptotic stability. *IEEE Trans. on Automatic Control*, 59(10), 2766–2771.

Rodriguez, J., Franquelo, L.G., Kouro, S., Leon, J.I., Portillo, R.C., Prats, M.A.M., and Perez, M.A. (2009). Multilevel converters: An enabling technology for high-power applications. *Proceedings of the IEEE*, 97(11), 1786–1817.

Rodríguez, J., Pontt, J., Kouro, S., and Correa, P. (2004). Direct torque control with imposed switching frequency in an 11-level cascaded inverter. *IEEE Trans. on Industrial Electronics*, 51(4), 827–833.

Sanfelice, R.G., Copp, D., and Nanez, P.A. (2013). A toolbox for simulation of hybrid systems in Matlab/Simulink: Hybrid equations (HyEQ) toolbox. In *Hybrid Systems: Computation and Control Conference.*

Senesky, M., Eirea, G., and Koo, T.J. (2003). Hybrid modelling and control of power electronics. In *International Workshop on Hybrid Systems: Computation and Control*, 450–465. Springer.

Serrani, A., Isidori, A., and Marconi, L. (2001). Semi-global nonlinear output regulation with adaptive internal model. *IEEE Transon Automatic Control*, 46(8), 1178–1194.

Sreekumar, C. and Agarwal, V. (2008). A hybrid control algorithm for voltage regulation in dc–dc boost converter. *IEEE Trans. on Industrial Electronics*, 55(6), 2530–2538.

Theunisse, T.A., Chai, J., Sanfelice, R.G., and Heemels, W.M.H. (2015). Robust global stabilization of the dc-dc boost converter via hybrid control. *IEEE Trans. on Circuits and Systems I: Regular Papers*, 62(4), 1052–1061.